■ Scientific Justification

Half of all galaxy clusters have an X-ray halo with a core cooling time $\ll H_0^{-1}$. These short cooling times should result in the formation of > 100 $M_\odot$ yr^{-1} "cooling flows" [see 32, for a review]. The continuum of X-ray gas temperatures expected in the cooling flow scenario are not observed [33, 40], and direct evidence for cooling flows, such as prodigious molecular cloud & star formation, are not found in the expected quantities [23, 27, 29]. Feedback from active galactic nuclei (AGN) has emerged as the consensus solution for regulating star formation and suppressing cooling of the hot halos of galaxies and clusters [3, 4, 10, 15]. Additionally, the existence of correlations between AGN outburst ages and host halo cooling times indicates the presence of a finely-tuned feedback loop [*i.e.* 5, 35]. But how AGN feedback energy is thermalized, specifically on scales the size of the host galaxy, and directed to gas with the shortest cooling times is still unclear [see 26, for a review]. Sparse observational evidence suggests weak shocks, sound waves, and conduction may be responsible [17, 20, 45].

It is well-known that conduction on its own has a minor role in defining galaxy cluster properties [14, 43]. But, when favorable magnetic field configurations are imposed by certain magnetohydrodynamic (MHD) processes [*e.g.* 2, 30], conduction is an efficient heating mechanism. In the presence of subsonic turbulence, for example from gentle mergers or AGN activity, numerical simulations have shown MHD processes can effectively boost conduction such that catastrophic cluster core cooling can be staved off [21, 31, 36]. One prediction of these simulations is that channels of preferentially radial magnetic fields are established within the cluster core. In the case of a cool core cluster, the radial fields connect regions of vastly different temperatures, thereby amplifying conductive heating between the regions. If these MHD processes function on galactic scales, then one may expect to find evidence for radial, conductively heated regions in cluster cores. This would serve as additional evidence that conduction has a vital role in distributing heat across the scales where rapid cooling is taking place.

To this end, BCG nebulae and optical filaments are a valuable diagnostic for understanding small-scale heating processes [7, 22, 28, 38, 44]. But only a handful of BCGs with *radial* optical filament systems have been studied in detail [9, 20, 28, 39]. Recently, Fabian et al. [18] demonstrated that the filaments around NGC 1275 must be magnetically supported, and Sparks et al. [40] suggested the detection of C IV, an efficient coolant at $\sim 10^5$ K, in one of M87's filaments results from conductive heating. Observational evidence is mounting that magnetism and conduction are important in explaining, and possibly regulating, the thermal state of BCG halos. But, better constraints are needed, and this requires deep, multiwavelength observations of cool core BCGs hosting radial optical filaments. One such object which is ideal for study is the extreme BCG IRAS 09104+4109 (hereafter IRAS09; $z = 0.4418$) which is the lowest redshift object demonstrating features of both radio- and quasar-modes of AGN feedback, and may be a local example of how massive galaxies at higher redshifts evolve from quasar-mode into radio-mode [6].

IRAS09 belongs to the population of uncommon low-redshift, ultraluminous infrared galaxies (ULIRG). Unlike nearly all ULIRGs, IRAS09 is the BCG in a rich galaxy cluster

with a strong cool core ($t_{\rm cool} < 0.3$ Gyr) which could supply the BCG with ample amounts of gas condensing out of the ICM ($\dot{M}_{\rm cool} > 500$ M$_\odot$ yr^{-1}). And unlike most BCGs, 99% of IRAS09's bolometric luminosity is emitted longward of 1 μm due to a heavily dust obscured Seyfert-2 [16, 24, 25]. However, while large amounts of hot dust and optical nebulae are detected in IRAS09, the galaxy hosts little cold dust and has no detected PAH features [11, 32, 37]. In addition, there are six compact spheroids within 50 kpc of the BCG which may be the bulges of cannibalized companions (shown in Figure 1). However, the BCG nebulae are not rotating relative to the galaxy, suggesting the nebulae were not stripped from companions [8]. But, the large dust content of the nebulae rules out the hot ICM as their origin due to short dust sputtering times in hot gas [12, 13]. IRAS09 also demonstrates features of a system having recently been in a "radio-mode" feedback but which is now clearly in a "quasar-mode" [Figure 1; 6]. The radio and cavity properties indicate a supersonic AGN outflow, but, the ionization state and dust fraction of gas neighboring the cavities indicate the nebulae are not being shock heated [42]. So, the origin, or more specifically, the physical, thermal, and emission properties, of the gas reservoir in IRAS09 is mysterious.

Utilizing *HST* WFPC2 imaging data, Armus et al. [1] pointed-out a series of red, tenuous, radially-oriented "whiskers" surrounding IRAS09 (Figure 1). The whiskers avoid the radio jet axis, which led Armus et al. [1] to suggest the whiskers might be cooling flow gas illuminated by QSO light escaping through "cracks" of the obscuring material. Our recent analysis of new Chandra and VLBA data [6] reveal that the nuclear emission is highly collimated away from the whiskers and leakage through a dusty torus would be insufficient to excite the level of emission seen in the whiskers. Thus, we suspect the whiskers are parts of giant radial Hα filaments ($l > 20$ kpc) similar to those seen around other BCGs. If so, then the morphologies and luminosities of the whiskers provide a sub-kpc probe of the magnetic and thermal state of BCG gas, and may provide further observational constraints on the influence of magnetism and conduction in cluster cores. **We propose to obtain deep, high-resolution near-infrared (NIR) and near-ultraviolet (NUV) observations of the IRAS 09104+4109 "whiskers" to determine their morphologies, composition, thermal & magnetic states, and to model the mechanisms which may be heating the whiskers.**

If the filament system in IRAS09 is comparable to those of other BCGs, then Hα emission (in the NIR for $z = 0.4418$) likely dominates the whisker flux. For a *WMAP* cosmology, the archival F814W *HST* data indicates the whiskers have widths $w < 450$ pc ($< 0.1''$) and lengths $l > 5700$ pc ($> 1''$), giving aspect ratios > 10. A combination of WFC3/IR and NICMOS/NIC1 observations will yield the flux measurements and spatial resolution, respectively, needed to calculate accurate Hα luminosities ($L_{\rm H\alpha}$) and more precise physical dimensions ($D_{\rm whk}$). Assuming a scaling between Hα luminosity and whisker gas mass, the whisker surface densities (Σ) can be derived from $D_{\rm whk}$ and $L_{\rm H\alpha}$. The magnetic field strengths, B, needed to explain the whisker morphologies in the presence of various forces (shear, gravity, internal turbulence, thermal pressure) are proportional to $C\Sigma^\alpha$, where C and α are functions of the various force assumptions. If the whiskers are thin, continuous objects, as in NGC 1275, then they are at a minimum stable against gravity, and the implied

B-field strengths along the whiskers need to be > 100 μG. For comparison, typical X-ray halo B-fields are of the order 1 μG. If the whisker fields are strong and associated with the ambient fields, then it suggests they have been amplified via some process, *e.g.* MHD amplification or AGN outflows stretching field lines. We point out that no whiskers are seen along the jet axis, suggesting some dynamical interaction between the whiskers and the AGN.

With a constraint on the whisker magnetic properties, the whisker thermal relationship with the ambient medium can be addressed. For example, if the whisker magnetic pressure dominates over the ambient thermal pressure, then simple contact heating at the whisker surfaces may be unlikely, and some other process(es), *e.g.* conduction along the B-fields, confined cosmic rays, gas phase mixing, massive star formation, or QSO irradiation, may be needed to explain the emission properties. We can also compare the whisker field strengths with those for magnetized relativistic jets. Might the whisker fields be the result of fields seeded by, or even coupled to on-going, AGN activity? Or, could the whiskers be glowing threads along magnetic loops emanating from the nucleus hosting the QSO? The on-going AGN outburst and (apparent) companion mergers in IRAS09 imply that the hot halo is turbulent. If the whiskers are magnetically dominated, that suggests the whiskers are coherent bodies, and interaction with the hot halo will be mostly kinematic. Thus, the whisker age upper limits can be derived, assuming a mean turbulent gas velocity, such that the B-fields resist whisker destruction by the ambient turbulent shear flows. Conversely, ages estimates from the whisker emission properties can be used to constrain the ambient turbulent velocities.

Equipped with measurements of the physical state of the whiskers, NUV continuum and line flux measurements with WFC3/UVIS and COS/NUV, respectively, will enable further interpretation of the whiskers' thermal state. Measurement, or upper limits, for whisker C IV line fluxes using COS/NUV spectroscopy, and NIR inferred densities & temperatures, will allow us to explore the parameter space of conductive heating models, for example with Cloudy [19], which can produce the observed C IV emission. The WFC3/UVIS imaging will map out the UV continuum in the COS/NUV passband, allowing us to constrain the contribution from star formation and AGN emission to our measurements for the whiskers. Further, if the whiskers are supported by strong, ordered B-fields, then they should be continuous, thin, mostly linear structures. However, if the NUV imaging in particular indicates the presence of knotty and diffuse emission, possibly from star formation, then this belies the influence of strong fields as the whisker gas should be mostly homogeneous.

Our proposed observations will also yield supplementary science regarding:
1) The UV emission line properties of the [O III] dominated ionized plume NE of the BCG.
2) The properties of the isolated filament ≈ 60 kpc NE of the BCG.
3) The nature of the six spheroids around IRAS09. Are they young rapidly star forming regions? Old, massive star clusters? Stripped bulges?
4) The finer details of the dusty gas obscuring the IRAS09 QSO.

Description of the Observations

NIR: Photometry using the archival F622W and F814W images indicate the whiskers are bluer than the nucleus and galaxy halo, but emit the strongest at redder wavelengths. Most of the whisker flux may be emerging as Hα emission at $\lambda_{\rm obs} = 9463$ Å. The whiskers have sizes $< 0.1''$ with other substructures being $0.2-0.5''$. The WFC3/IR (resolution $0.13''$/pixel) field of view (FOV) and F098M filter throughput are larger than the NICMOS/NIC1-F090M in the NIR, but the angular resolution of NIC1 ($0.04''$/pixel) is required to resolve the whiskers. **We therefore request 3 orbits for our NIR science objectives: 0.75 orbits with WFC3/IR for flux measurements and 2.25 orbits with NICMOS/NIC1 to resolve structure.**

For comparison, the F622W and F814W passbands of the archival observations are shown with the F090M and F098M passbands of the proposed observations in Figure 2. Our proposed observations are longward of [O III] emission and will not be affected by the bright [O III] BCG nebulae. The IRAS09 SED peaks longward of 2 μm, the end of the WFC3/IR-F098M passband, and contamination from hot dust should be minimal. Cold dust contributes $< 3\%$ of $L_{\rm bol}$ in IRAS09 [11] further maximizing the detectability of Hα between 0.8-1.1 μm. The Hα contribution to the F098M and F090M filters was estimated using the Hβ equivalent width (EW) of the NE [O III] plume provided in Tran et al. [42]. Assuming a dereddend Balmer decrement of 3, and that 40% of the whisker fluxes arise from Hα, the Hα(EW) to F090M(EW) & F098M(EW) ratios are $\approx 15-20\%$, which is a lower limit given that the whiskers may be Hα dominated relative to the [O III] plume and that they cover a larger area. The WFC3/IR F098M and NIC1 F090M filters provide sufficient wavelength coverage and transmission to make Hα emission a dominant feature in the imaging.

To determine needed exposure times, we treat IRAS09 as an extended ($R = 5''$), Galactic-reddened, redshifted elliptical galaxy with emission lines at Hβ 4865 Å, [O III], and [Fe VII] 8776 Å (fluxes provided in Tran et al. [42]). The galaxy template was flux normalized using the SDSS-z detection (0.492 mJy at 0.921 μm), and standard average backgrounds were added. With the WFC3/IR-F098M setup, a 900 s exposure ($3/5^{\rm th}$ the saturation time) gives a signal-to-noise ratio (SN) of ~ 200 for a 0.13 arcsec^2 extraction region. This will enable flux measurements to ± 0.08 mag and, assuming the F814W stellar continuum to whisker flux ratio scales linear into the F098M passband, the whiskers should have average contrasts with the galaxy of ≈ 1.2 mag. Using the same galaxy template, for the NICMOS/NIC1-F090M setup, a 6700 s exposure ($1/20^{\rm th}$ of the saturation time) yields a SN of 50 for a 0.13 arcsec^2 extraction region. This will be sufficient to resolve whisker detail at the resolution limit of the NIC1 instrument.

Our science goals in the NIR can be achieved in 3 orbits. At $+41^\circ$ declination, one orbit has 57 min of observable time. For the first orbit, the NIC1 overhead plus setup time is ≈ 7 m, and ≈ 5 min for subsequent orbits. To achieve the 112 min of NIC1 science exposure time requires 2.25 orbits. Changing to WFC3/IR in the third orbit requires 10 min for spacecraft maneuvering, setup, and overhead. A WFC3/IR science exposure of 15 min leaves 17 min

in the third orbit.

NUV: Imaging BCG and filament UV emission requires the high throughput and angular resolution of WFC3/UVIS (resolution 0.04″/pixel). Unambiguous detection of the C IV resonant line ($\lambda_{\rm obs} = 2233$ Å) to constrain conductive heating models for the filaments requires the dispersive resolution and sensitivity of the COS/NUV spectrograph. **We therefore request 10 orbits to achieve our NUV science objectives: 2.4 orbits with WFC3/UVIS to map spatial emission, and 7.6 orbits with COS/NUV to, at a minimum, place tight upper limits on C IV emission.**

The C IV line falls near the peak of the WFC3/UVIS-F218W filter and is one of the available central wavelengths of the COS/NUV-G225M grating. To assist our exposure time calculations, we simulated the expected spectrum of a conductively heated gas slab in Cloudy with the dimensions of the whiskers and density of the NE [O III] plume as a calibrator. Summing over the number of predicted whiskers and their sky area, we predict a C IV flux of $\sim 6 \times 10^{-14}$ erg s^{-1} cm^{-2}. The next brightest line within the F218W passband has 25% of the C IV flux and falls outside of the dispersion windows of the G225M grating.

Assuming the model fluxes are accurate, a COS/NUV exposure time was calculated to reach a SN per resolution element of 4 at 2233 Å, which should be sufficient to provide $\gtrsim 3\sigma$ line detection at the dispersion limit of COS/NUV. For the COS/NUV-G225M setup, we set $\lambda_{\rm cent} = 2233$ Å with a Galactic-reddened, redshifted elliptical galaxy with an emission line at 2233 Å. The galaxy template was flux normalized using the *GALEX* NUV detection ($m = 19.58$ mag) with standard average backgrounds assumed. The required exposure time is 20160 sec. For the first orbit, the total COS/NUV overhead and setup time is 9 min with 8 min for subsequent orbits. The science exposure time then requires 7.6 orbits to complete. A WFC3/UVIS exposure time was calculated for the WFC3/UVIS-F218W setup with a goal of attaining a SN of 15 per pixel. The same galaxy template was used as for the spectroscopy. The required exposure time is 6732 sec ($\ll 1\%$ of the saturation time). Alloting for spacecraft maneuvering and 5 min of WFC3/UVIS overhead & setup times, the science exposures can be achieved in 2.4 orbits, bringing our total request to 10 orbits.

The requested target field does not contain excessively bright UV sources that might damage the WFC3/UVIS or COS/NUV instruments. The COS/NUV Bright Object Protection policies require that count rates not exceed a global limit of 30000 ct/s/stripe and local limit of 70 ct/s/pixel. The requested COS/NUV exposures yield a global rate of 85 ct/s, a local rate of $\ll 1$ ct/s, and no stripe exceeding 5.5 ct/s. The count rate during target acquisition imaging does not exceed the 300 ct/s limit in a 9×9 pixel region around the target. No brightness-related limits are imposed for WFC3/UVIS.

The NIR observations have the highest priority and would achieve many of our scientific goals. If the TAC decided not to award the NUV requests, specifically the COS spectroscopy, our ability to model and constrain conductive heating of the filaments will be very limited. However, NIR imaging of the BCG inner regions will further resolve the structure of gas which dominates $L_{\rm bol}$ and enable us to place interesting constraints on the AGN-environment interaction which will be worthy of publication.

Special Requirements

Coordinated Observations

Justify Duplications

Past HST Usage and Current Commitments

References

[1] Armus et al., Ap&SS, 266:113-118, 1999
[2] Balbus, ApJ 534:420-427, May 2000
[3] Bîrzan et al. ApJ, 607:800-809, June 2004
[4] Bower et al. MNRAS, 390:1399-1410, November 2008
[5] Cavagnolo et al. ApJ, 683:L107-L110, August 2008
[6] Cavagnolo et al. ApJ submitted, 2010
[7] Conselice et al. AJ, 122:2281-2300, November 2001
[8] Crawford & Vanderriest. MNRAS, 283:1003-1014, December 1996
[9] Crawford et al. MNRAS, 363:216-222, October 2005
[10] Croton et al. MNRAS, 365:11-28, January 2006
[11] Deane & Trentham. MNRAS, 326:1467-1474, October 2001
[12] Donahue & Voit. ApJ, 414:L17-L20, September 1993
[13] Draine & Salpeter. ApJ, 231:77-94, July 1979
[14] Dunn & Fabian. MNRAS, 385:757-768, April 2008
[15] Dunn et al. MNRAS, 364:1343-1353, December 2005
[16] Evans et al. ApJ, 506:205-221, October 1998
[17] Fabian et al. MNRAS, 366:417-428, February 2006
[18] Fabian et al. Nature, 454:968-970, August 2008
[19] Ferland et al. PASP, 110:761-778, July 1998
[20] Forman et al. ApJ, 665:1057-1066, August 2007
[21] Guo et al. ApJ, 688:859-874, December 2008
[22] Hatch et al. MNRAS, 380:33-43, September 2007
[23] Heckman et al. ApJ, 338:48-77, March 1989
[24] Hines & Wills. ApJ, 415:82-+, September 1993
[25] Kleinmann et al. ApJ, 328:161-169, May 1988
[26] McNamara & Nulsen. ARA&A, 45:117-175, September 2007
[27] McNamara et al. ApJ, 360:20-29, September 1990
[28] McDonald et al. ApJ, 721:1262-1283, October 2010
[29] O'Dea et al. ApJ, 422:467-479, February 1994
[30] Parrish & Quataert. ApJ, 677:L9-L12, April 2008
[31] Parrish et al. ApJ, 703:96-108, September 2009

[32] Peeters et al. ApJ, 613:986-1003, October 2004
[33] Peterson & Fabian. Phys. Rep., 427:1-39, April 2006
[34] Peterson et al. ApJ, 590:207-224, June 2003
[35] Rafferty et al. ApJ, 687:899-918, November 2008
[36] Ruszkowski & Oh. ArXiv e-prints: 0911.5198, November 2009
[37] Sargsyan et al. ApJ, 683:114-122, August 2008
[38] Sparks et al. ApJ, 345:153-162, October 1989
[39] Sparks et al. ApJ, 607:294-301, May 2004
[40] Sparks et al. ApJ, 704:L20-L24, October 2009
[41] Tamura et al. A&A, 365:L87-L92, January 2001
[42] Tran et al. AJ, 120:562-574, August 2000
[43] Voigt & Fabian. MNRAS, 347:1130-1149, February 2004
[44] Voit & Donahue. ApJ, 486:242-+, September 1997
[45] Voit et al. ApJ, 681:L5-L8, July 2008.

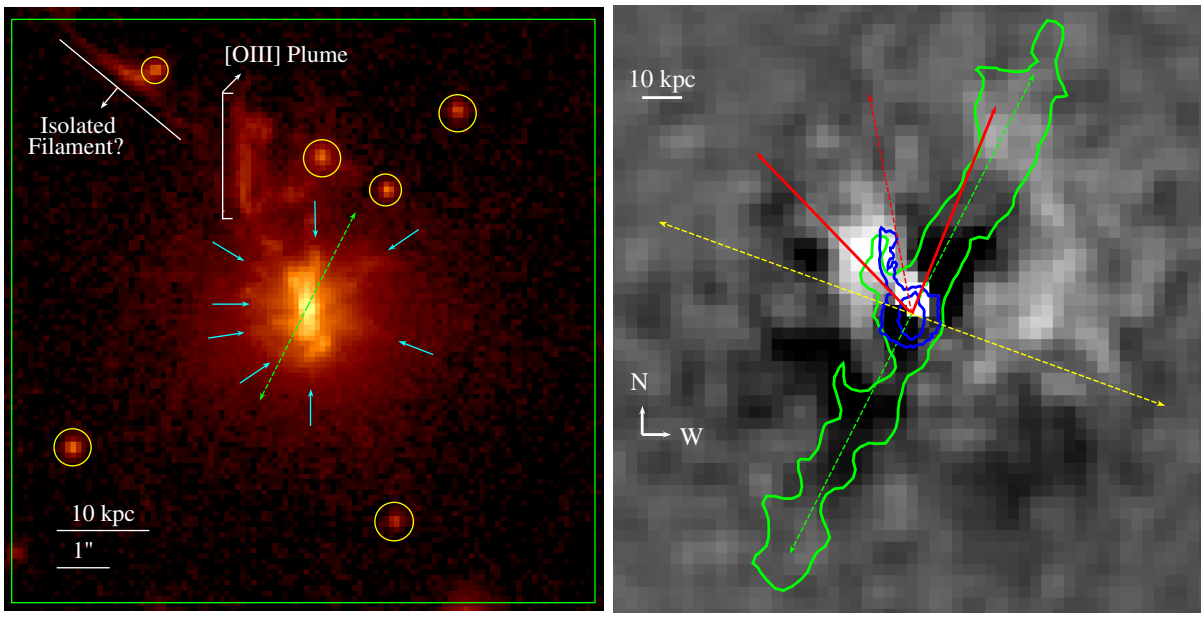

Figure 1: **Left:** Rest-frame 4910-6650 Å *HST* image of the IRAS09 BCG. Green box denotes the NIC1 FOV; cyan arrows highlight "whiskers," yellow circles enclose (stellar?) spheroids; green dashed line marks AGN axis. **Right**: *Chandra* residual 0.5-10.0 keV X-ray image. Green contour & dashed line show VLA 1.4 GHz radio emission and jet axis, respectively; blue contours trace rest-frame 3900-4570 Å *HST* image (the extension is the NE [O III] plume); red solid lines denote opening angle of QSO ionization cone; yellow dashed line indicates dark matter halo major-axis.

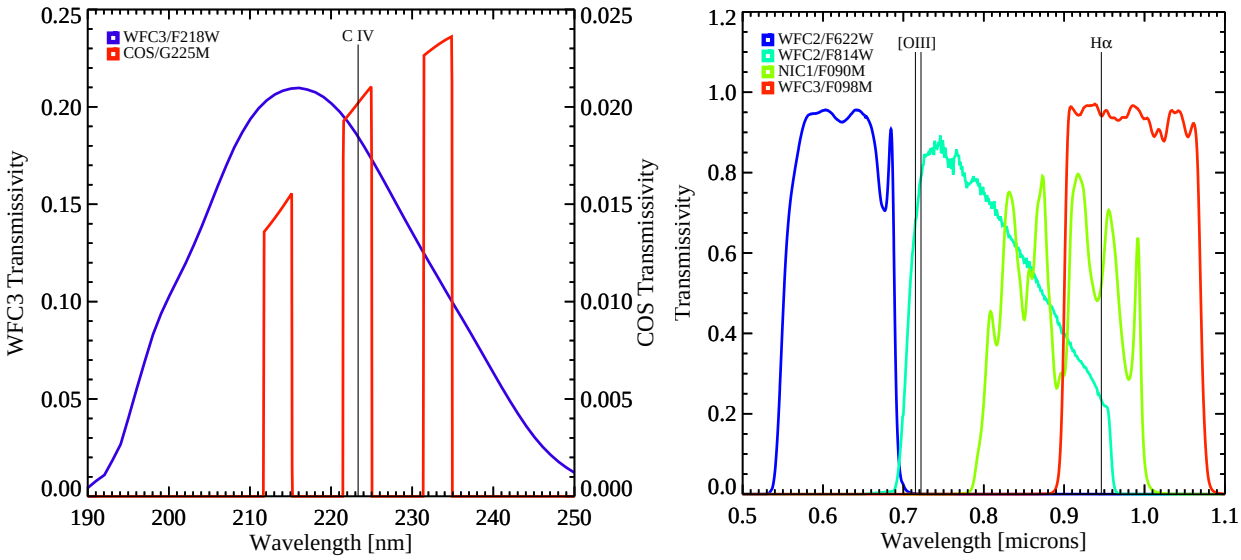

Figure 2: Comparison of passbands with relevant emission lines labeled. **Left:** Proposed NUV imaging and spectroscopy. **Right:** Archived optical and proposed NIR observations.